

Lecture Notes in Physics

Founding Editors: W. Beiglböck, J. Ehlers, K. Hepp, H. Weidenmüller

Editorial Board

R. Beig, Vienna, Austria
W. Beiglböck, Heidelberg, Germany
W. Domcke, Garching, Germany
B.-G. Englert, Singapore
U. Frisch, Nice, France
P. Hänggi, Augsburg, Germany
G. Hasinger, Garching, Germany
W. Hillebrandt, Garching, Germany
R. L. Jaffe, Cambridge, MA, USA
W. Janke, Leipzig, Germany
H. v. Löhneysen, Karlsruhe, Germany
M. Mangano, Geneva, Switzerland
J.-M. Raimond, Paris, France
D. Sornette, Zurich, Switzerland
S. Theisen, Potsdam, Germany
W. Weise, Garching, Germany
J. Zittartz, Köln, Germany

The Lecture Notes in Physics

The series Lecture Notes in Physics (LNP), founded in 1969, reports new developments in physics research and teaching – quickly and informally, but with a high quality and the explicit aim to summarize and communicate current knowledge in an accessible way. Books published in this series are conceived as bridging material between advanced graduate textbooks and the forefront of research and to serve three purposes:

- to be a compact and modern up-to-date source of reference on a well-defined topic
- to serve as an accessible introduction to the field to postgraduate students and nonspecialist researchers from related areas
- to be a source of advanced teaching material for specialized seminars, courses and schools

Both monographs and multi-author volumes will be considered for publication. Edited volumes should, however, consist of a very limited number of contributions only. Proceedings will not be considered for LNP.

Volumes published in LNP are disseminated both in print and in electronic formats, the electronic archive being available at springerlink.com. The series content is indexed, abstracted and referenced by many abstracting and information services, bibliographic networks, subscription agencies, library networks, and consortia.

Proposals should be sent to a member of the Editorial Board, or directly to the managing editor at Springer:

Christian Caron
Springer Heidelberg
Physics Editorial Department I
Tiergartenstrasse 17
69121 Heidelberg / Germany
christian.caron@springer.com

N. Akhmediev
A. Ankiewicz (Eds.)

Dissipative Solitons: From Optics to Biology and Medicine

 Springer

Nail Akhmediev
Australian National University
Optical Sciences Center
Canberra ACT 0200
Australia
nna124@rsphy1.anu.edu.au

Adrian Ankiewicz
Australian National University
Optical Sciences Center
Canberra ACT 0200
Australia
ana124@rsphy1.anu.edu.au

Akhmediev, N., Ankiewicz, A.(Eds.), *Dissipative Solitons: From Optics to Biology and Medicine*, Lect. Notes Phys. 751 (Springer, Berlin Heidelberg 2008), DOI 10.1007/978-3-540-78217-9

ISBN: 978-3-540-78216-2

e-ISBN: 978-3-540-78217-9

DOI 10.1007/978-3-540-78217-9

Lecture Notes in Physics ISSN: 0075-8450

Library of Congress Control Number: 2008922888

© 2008 Springer-Verlag Berlin Heidelberg

This work is subject to copyright. All rights are reserved, whether the whole or part of the material is concerned, specifically the rights of translation, reprinting, reuse of illustrations, recitation, broadcasting, reproduction on microfilm or in any other way, and storage in data banks. Duplication of this publication or parts thereof is permitted only under the provisions of the German Copyright Law of September 9, 1965, in its current version, and permission for use must always be obtained from Springer. Violations are liable to prosecution under the German Copyright Law.

The use of general descriptive names, registered names, trademarks, etc. in this publication does not imply, even in the absence of a specific statement, that such names are exempt from the relevant protective laws and regulations and therefore free for general use.

Cover design: xxxx

Printed on acid-free paper

9 8 7 6 5 4 3 2 1

springer.com

Contents

Three Sources and Three Component Parts of the Concept of Dissipative Solitons	1
N. Akhmediev and A. Ankiewicz	
Solitons in Viscous Flows	29
M.G. Velarde and A.A. Nepomnyashchy	
Cavity Solitons in Semiconductor Devices	51
L.A. Lugiato, F. Prati, G. Tissoni, M. Brambilla, S. Barland, M. Giudici, and J.R. Tredicce	
Dissipative Solitons in Laser Systems with Non-local and Non-instantaneous Nonlinearity	93
N.N. Rosanov, S.V. Fedorov, and A.N. Shatsev	
Excitability Mediated by Dissipative Solitons in Nonlinear Optical Cavities	113
P. Colet, D. Gomila, A. Jacobo, and M.A. Matías	
Temporal Soliton “Molecules” in Mode-Locked Lasers: Collisions, Pulsations, and Vibrations	137
P. Grelu and J.M. Soto-Crespo	
Compounds of Fiber-Optic Solitons	175
F. Mitschke	
Dissipative Nonlinear Structures in Fiber Optics	195
S.K. Turitsyn and S. Boscolo	
Three-Wave Dissipative Brillouin Solitons	221
C. Montes	

Spatial Dissipative Solitons Under Convective and Absolute Instabilities in Optical Parametric Oscillators	261
S. Coulibaly, C. Durniak, and M. Taki	
Discrete Breathers with Dissipation	289
S. Flach and A.V. Gorbach	
Anharmonic Oscillations, Dissipative Solitons and Non-Ohmic Supersonic Electric Transport	321
M.G. Velarde, W. Ebeling, and A.P. Chetverikov	
Coherent Optical Pulse Dynamics in Nano-composite Plasmonic Bragg Gratings	337
I.R. Gabitov, A.O. Korotkevich, A.I. Maimistov, and J.B. McMahon	
Collective Focusing and Modulational Instability of Light and Cold Atoms	361
M. Saffman and Y. Wang	
On Vegetation Clustering, Localized Bare Soil Spots and Fairy Circles . . .	381
M. Tlidi, R. Lefever, and A. Vladimirov	
Propagation of Traveling Pulses in Cortical Networks	403
D. Golomb	
Wave Phenomena in Neuronal Networks	431
W.C. Troy	
Spiral Waves and Dissipative Solitons in Weakly Excitable Media	453
V.S. Zykov	
Index	475

Excitability Mediated by Dissipative Solitons in Nonlinear Optical Cavities

P. Colet, D. Gomila, A. Jacobo, and M.A. Matías

Abstract Cavity solitons, which are dissipative solitons with a finite extension that appear in the transverse plane of nonlinear optical cavities, have been advocated for use in fast and compact optical information storage. We discuss the instabilities that can affect cavity solitons appearing in Kerr cavities. In particular, cavity solitons may exhibit a Hopf bifurcation leading to self-pulsating behavior, which is then followed by the destruction of the oscillation in a saddle-loop bifurcation. Beyond this point, there is a regime of excitable cavity solitons which appear when suitable perturbations are applied. Excitability is characterized by the nonlinear response of the system upon the application of an external stimulus. Only stimuli exceeding a threshold value are able to elicit a full and well-defined response in the system. In the case of cavity solitons, excitability emerges from the spatial dependence, since the system does not exhibit any excitable behavior locally. We demonstrate the existence of two different mechanisms which lead to excitability, depending on the profile of the pump field.

P. Colet

Instituto Mediterráneo de Estudios Avanzados IMEDEA (CSIC-UIB), Campus Universitat de les Illes Balears, E-07122 Palma de Mallorca, Spain, pere@imedea.uib.es

D. Gomila

Instituto Mediterráneo de Estudios Avanzados IMEDEA (CSIC-UIB), Campus Universitat de les Illes Balears, E-07122 Palma de Mallorca, Spain, damia@imedea.uib.es

A. Jacobo

Instituto Mediterráneo de Estudios Avanzados IMEDEA (CSIC-UIB), Campus Universitat de les Illes Balears, E-07122 Palma de Mallorca, Spain, jacobo@imedea.uib.es

M.A. Matías

Instituto Mediterráneo de Estudios Avanzados IMEDEA (CSIC-UIB), Campus Universitat de les Illes Balears, E-07122 Palma de Mallorca, Spain, manuel@imedea.uib.es

Colet, P. et al.: *Excitability Mediated by Dissipative Solitons in Nonlinear Optical Cavities*. Lect. Notes Phys. **751**, 113–135 (2008)
DOI 10.1007/978-3-540-78217-9_5

© Springer-Verlag Berlin Heidelberg 2008

1 Introduction

The concept of excitability was initially introduced in the context of biological systems, e.g., to describe neuron firing, and it has been found to be present in a wide variety of systems [1, 2], including optical systems [3, 4, 5, 6, 7]. Typically, a system is considered to be excitable if the response of the system to perturbations of the stationary state varies greatly, depending on whether the amplitude of the perturbation exceeds a threshold value. Thus, while small perturbations induce a smooth return to the fixed point, above-threshold perturbations induce a large phase space excursion (firing) before coming back to the rest state. Furthermore, after one firing, the system cannot be excited again within a refractory period of time. In phase space [8, 9], excitability occurs for parameter regions where a stable fixed point is close to a bifurcation in which an oscillation is created. A well-known example of an excitable system is the FitzHugh–Nagumo model, close to the Hopf bifurcation. One may also find excitable behavior mediated by a saddle point, in the form of either an Andronov (or saddle node on the invariant circle) bifurcation or a saddle-loop (or homoclinic) bifurcation. These three scenarios are the simplest possible, and they occur in systems that, minimally, can be characterized by two phase space variables. The first scenario is characterized by the fact that the response time to come back to the fixed point after a firing is basically constant. This is described as a Class II excitability. In the last two scenarios, where excitability is mediated by a saddle, the distribution of response times is unbounded and they are described as Class I excitability.

The concept of excitability has been extended to systems with spatial dependence by coupling several or many zero-dimensional excitable systems [1, 2]. Here, we consider a different situation – a system that does not show excitable behavior when there is no spatial dependence, but does show this behavior when the dissipative localized structures appear in an extended system with spatial dependence.

Dissipative solitons (DSs) are spatially localized structures that appear in certain dissipative media [10, 11], and, in particular, they have been found in a variety of systems, including chemical reactions [12, 13], gas discharges [14], and fluids [11]. They are also found in optical cavities due to the interplay of different effects, such as diffraction, nonlinearity, driving, and dissipation [15, 16, 17, 18, 19]. These structures, also known in this field as cavity solitons, have to be distinguished from conservative solitons which are found, for example, in propagation in fibers, and for which there is a continuous family of solutions, which can depend on the initial conditions. Instead, a cavity soliton is unique once the parameters of the system have been fixed. This fact makes these structures potentially useful in optical (i.e., fast and spatially dense) storage and processing of information [17, 19, 20, 21, 22].

DSs may develop various kinds of instabilities, as they may start moving, breathing, or oscillating. In the latter case, the amplitude of the DS oscillates in time, while its position remains stationary in space, like the “oscillons” found in a vibrating layer of sand [23]. Oscillating DSs are autonomous oscillons and have been reported in both optical [24, 25, 26] and chemical systems [27]. They appear when the DS exhibits a Hopf bifurcation. Here, we describe a route by which autonomous

oscillating DSs are destroyed, leading to an excitability regime [28, 29]. The excitable behavior may confer new computational capabilities, beyond information storage, to DSs in optical systems.

In particular, we consider the dynamics of DSs arising in optical cavities filled with a Kerr nonlinear medium. These are known as Kerr cavity solitons (KCS) as a consequence of a modulational (namely a pattern-forming) instability of a homogeneous solution. They exist in the parameter range where the homogeneous solution coexists with sub-critical (hexagonal) patterns. They share some properties with propagating spatial (conservative) solitons in a Kerr medium, but there are also interesting differences. While Kerr spatial solitons are stable in one transverse dimension (1D), it is well known that their 2D counterparts are unstable against self-focusing collapse [30]. The stability and dynamics of 2D Kerr cavity solitons are thus of particular interest, and their existence and stability have been studied in several papers [24, 25, 31].

Here, we show the existence of different mechanisms leading to excitability, depending on the profile of the pump field. For a homogeneous pump, the mechanism leading to excitable behavior is a saddle-loop bifurcation through which a stable oscillating DS collides with an unstable DS [28, 29]. For a system pumped by a localized Gaussian beam on top of a homogeneous background, the scenario is richer and one finds two different mechanisms leading to excitability. One is based on a saddle-loop bifurcation, as above, while the other takes place through a saddle node in an invariant circle (SNIC) bifurcation. Under the second mechanism, the excitability threshold can be tuned by changing accessible system parameters.

2 Model

An optical cavity filled with a nonlinear Kerr medium can be described by the model introduced by Lugiato and Lefever [32]. This prototype model, obtained by averaging the dependence of the field along the propagation direction, was first introduced to study pattern formation in this system. Later studies showed that this model also exhibits DSs in some parameter regions [24, 31]. In the paraxial limit, after suitably rescaling the variables, the dynamics of the intra-cavity slowly varying amplitude of the electromagnetic field $E(\mathbf{x}, t)$, where $\mathbf{x} = (x, y)$ is the plane transverse to the propagation direction, is given by

$$\frac{\partial E}{\partial t} = -(1 + i\theta)E + i\nabla^2 E + E_1 + i|E|^2 E. \quad (1)$$

The first term on the right-hand side describes cavity losses (which make the system dissipative), E_1 is the input field, θ the cavity detuning with respect to E_1 , and $\nabla^2 = \partial^2/\partial x^2 + \partial^2/\partial y^2$ is the transverse Laplacian which models diffraction. The sign of the cubic term indicates the so-called self-focusing case.

When neither loss nor input field is present, the intra-cavity field can be rescaled to $E \rightarrow E e^{i\theta t}$ to remove the detuning term and (1) becomes the nonlinear Schrödinger

equation (NLSE). For the NLSE in two spatial dimensions, an initial condition with sufficient energy collapses, so energy accumulates at a point in space, leading to the divergence of the solution at a finite time [33]. Dissipation, such as that originating from the cavity losses, can prevent this collapse [34]. In any case, in the parameter region in which DSs are stable, their dynamics is closely related to the collapse regime. In our system, the above mechanism, which combines collapse and cavity losses, is also responsible for various instabilities arising in regular patterns which lead to complex spatio-temporal dynamical behavior, including the existence of optical turbulence [35].

Firstly, we will consider the case in which the input field is homogeneous, viz. $E_1(\mathbf{x}) = E_0$. In Sect. 10, we address the case in which the pump consists of a localized Gaussian beam on top of a homogeneous background. For a constant pump, Equation (1) has a homogeneous steady-state solution which is implicitly given by $E_s = E_0/(1 + i(\theta - I_s))$, where $I_s = |E_s|^2$ [32]. For convenience, we will use the intra-cavity background, I_s , together with θ , as our control parameters. It is well known that the homogeneous solution shows bistability for $\theta > \sqrt{3}$.

In the following sections, it is convenient to introduce the field $A(x, y)$ as $E = E_s(1 + A)$, so that $A(x, y)$ describes the solution without the homogeneous background. Equation (1) can be rewritten as

$$\frac{\partial A}{\partial t} = -(1 + i\theta)A + i\nabla^2 A + iI_s(2A + A^* + A^2 + 2|A|^2 + |A|^2 A). \quad (2)$$

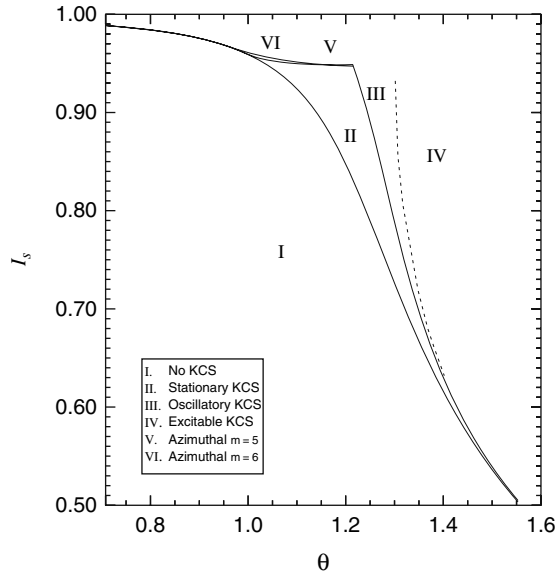
Note that this equation is fully equivalent to (1), without any linear approximation.

For numerical simulations, we integrate (1) using a pseudo-spectral method where the linear terms in Fourier space are integrated exactly, while the nonlinear ones are integrated using an approximation which is second order in time [29, 36]. Periodic boundary conditions are used since they are convenient for the pseudo-spectral code. The system size is large enough to ensure that the electric field reaches the homogeneous steady state well inside the boundaries. A square lattice of size 512×512 points was used. The space discretization was taken as $dx = 0.1875$, while the time step was $dt = 10^{-3}$.

3 Dissipative Solitons for Homogeneous Pump

The homogeneous solution is stable for $I_s < 1$. The so-called modulation instability takes place at $I_s = 1$ and the homogeneous solution becomes unstable, leading to the formation of hexagonal patterns [32, 37]. For $I_s > 1$, the homogeneous solution continues to exist, although it is unstable. The hexagonal patterns are sub-critical, viz. through an S-shaped branch, and thus, they coexist with the stable homogeneous solution for a certain parameter range. This bistability is at the origin of the existence of stable DSs that appear when suitable (localized) transient perturbations are applied. The DS can be seen as a solution connecting a cell of the pattern with the

Fig. 1 Phase diagram of DSs in a Kerr cavity. KCSs are stable in region II and oscillate in III. (The line between these two regions indicates a Hopf bifurcation.) In the lower part, below the saddle-node bifurcation (*solid line*), there are no KCSs. When crossing from regions III to V (VI), one KCS develops azimuthal instabilities, with $m = 5$ ($m = 6$) which lead to an extended pattern. To the left of the saddle-loop bifurcation (*dashed line*), the system exhibits excitability



homogeneous solution. While the existence of DSs in this bistable regime is quite generic in extended systems, the stability of such DSs strongly depends on the particular system. The region of existence of DSs, also known as Kerr cavity solitons (KCSs), in parameter space is shown in Fig. 1 [25].

The mechanism by which KCSs appear is a saddle-node (or fold) bifurcation, as can be seen in Fig. 2 for $\theta = 1.34$ and $I_s \sim 0.655$ ($|E_0|^2 \sim 4.5$), where a pair of stable–unstable DSs are created [21, 38]. The middle-branch KCS is unstable and ends at the modulational instability point where it collides with the homogeneous solution. The middle-branch KCS then acts as a barrier. Thus, if an initial condition is somewhat above the middle branch in phase space, it will evolve to the upper branch (so that a DS is written), while it will decay to the homogeneous solution if below it. This role of the middle-branch DS, as a separatrix in phase space, is quite general and has been identified in a semiconductor model [39] and experimentally observed for solitons in a sodium cell with feedback [40, 41, 42] and in a semiconductor cavity [43].

The DSs are rotationally symmetric about their centers. Figure 2 shows the spatial shape of a typical upper- and middle-branch DS. The transverse profile can be accurately found by taking advantage of the symmetry. From (2), one obtains the radial equation for $A(r)$:

$$\begin{aligned} \frac{\partial A}{\partial t} = & -(1 + i\theta)A + i \left(\frac{\partial^2}{\partial^2 r} + \frac{1}{r} \frac{\partial}{\partial r} \right) A \\ & + iI_s (2A + A^* + A^2 + 2|A|^2 + |A|^2 A). \end{aligned} \quad (3)$$

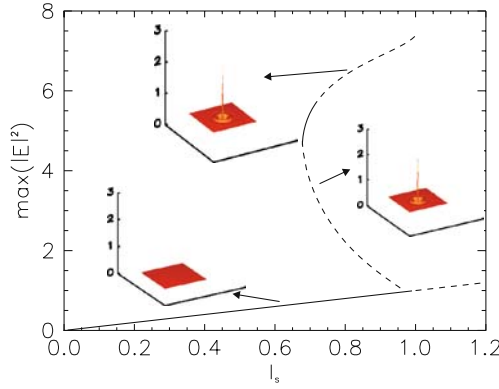


Fig. 2 Bifurcation diagram of stationary KCSs: $\max(|E|^2)$ vs. I_s for $\theta = 1.34$. *Solid lines* represent stable solutions and *dashed lines* unstable ones. The lowest branch corresponds to the homogeneous solution that becomes unstable at $I_s = 1.0$. The upper branch corresponds to the stable KCS, while the middle branch corresponds to the unstable KCS. Upper and middle branches originate at the saddle-node bifurcation. The upper branch becomes Hopf unstable for larger values of I_s . The 3D plots, from top to bottom, show the profiles of the upper-branch KCSs, the middle-branch KCSs, and the homogeneous solution

Steady-state DS solutions, both stable and unstable, are found by equating the left-hand side of (3) to zero. The boundary conditions for this problem are such that the derivatives are zero at the boundaries: $\partial A / \partial r(r=0) = \partial A / \partial r(r=L) = 0$, where the system size, L , is large enough to ensure that the electric field smoothly approaches the homogeneous solution ($A(r) \rightarrow 0$) before reaching the boundary. Discretizing the radial coordinate, one obtains a set of coupled nonlinear equations which can be solved using a Newton–Raphson method [44, 45]. Spatial derivatives are computed in Fourier space. The initial guess for the Newton method is obtained from a radial cut of a numerical integration of the 2D equation (1). After obtaining a precise solution for given parameter values, continuation techniques [46] are used to explore the region of existence of KCSs in the parameter space. This approach is extremely accurate, and it allows us to find both stable and unstable fixed point solutions.

The stability of the DS against radial and azimuthal perturbations is obtained, cf. [47], by linearizing equation (2) around the stationary DS, $A_{DS}(r)$. This yields a linearized equation for the time evolution of the perturbations $\delta A(r, \phi, t) = A(r, \phi, t) - A_{DS}(r)$. The solutions of the linear problem can be written as

$$\delta A = [R_+(r) e^{im\phi} + R_-(r) e^{-im\phi}] \exp(\lambda t), \quad (4)$$

where m is the wavenumber of the azimuthal perturbation. This yields the eigenvalue problem

$$\mathbf{U}\Psi = \lambda\Psi, \quad (5)$$

where $\Psi = (R_+, R_-^*)^\top$ and $\mathbf{U} = \begin{pmatrix} U_+ & U_- \\ U_-^* & U_+^* \end{pmatrix}$ with

$$\begin{aligned}
U_+ &= -(1 + i\theta) + i \left(\frac{\partial^2}{\partial^2 r} + \frac{1}{r} \frac{\partial}{\partial r} - \frac{m^2}{r^2} \right) + i2I_s (1 + A_{\text{DS}} + A_{\text{DS}}^* + |A_{\text{DS}}|^2) \\
U_- &= iI_s (1 + 2A_{\text{DS}} + A_{\text{DS}}^2) .
\end{aligned} \tag{6}$$

For purely radial perturbations ($m = 0$), we have $R_- = R_+$. The matrix \mathbf{U} is time independent, as it is evaluated at the stationary DS (stable or unstable) under study.

The problem thus reduces to finding the eigenvalues, λ , and eigenvectors, Ψ , where it is important to mention that \mathbf{U} is a complex matrix, so the eigenvectors are, in general, complex quantities. Due to the symmetry of \mathbf{U} , the eigenvalues are either real or pairs of complex conjugates. This last property stems from the fact that, considering the real and imaginary parts of A_s , \mathbf{U} can be rewritten as a real matrix. Due to the discretization of the space, Ψ becomes a vector whose dimension is $2N$. The set of eigenvectors Ψ_i ($i = 1, 2N$) forms a basis, and their amplitudes define a natural phase space for studying the dynamics of DSs. Thus, the stability problem of stationary DSs, which, in principle, live in an infinite-dimensional phase space, is numerically reduced to the study of these stationary DSs in a finite, albeit large, dimensional phase space. However, we note that \mathbf{U} is not self-adjoint, and these modes do not form an orthogonal basis. To find the components of a field profile on a mode Ψ_i , one has to project it onto the corresponding eigenmode Φ_i of the adjoint Jacobian matrix \mathbf{U}^\dagger .

The stability of the 2D KCS, as function of the two control parameters (θ, I_s) , is displayed in Fig. 1. The lowest curve corresponds to the saddle-node bifurcation where the upper and middle KCS branches collide. There are no KCS solutions below this line. The area above the saddle-node curve shows where 2D KCSs exist, and region II corresponds to the parameter values for which they are stable. For a given detuning, KCSs only exist for a finite range of background intra-cavity intensities, $I_{\text{min}} < I_s < 1$. While the range of existence is broader when the detuning is increased, the range in which KCSs are stable is, in fact, narrower. For $\theta > 1.5$, it is so narrow that early studies missed the existence of stable KCSs altogether [31]. DSs can be unstable to perturbations at zero azimuthal number ($m = 0$), when crossing from regions II to III in Fig. 1, or to azimuthal perturbations ($m \neq 0$), when crossing from II to V or VI [25]. In the first case, the instability preserves the shape of the KCS and leads to an oscillatory DS. This case will be discussed in detail in Sect. 5. On the other hand, when the KCS undergoes an azimuthal instability, its radial symmetry is broken and a pattern arises, as discussed in the next section.

4 Azimuthal Instabilities

For the approximate range $\theta < 1.22$, shown in Fig. 1, the KCS become unstable as I_s is increased due to an azimuthal instability with $m = 5$ or $m = 6$, depending on the

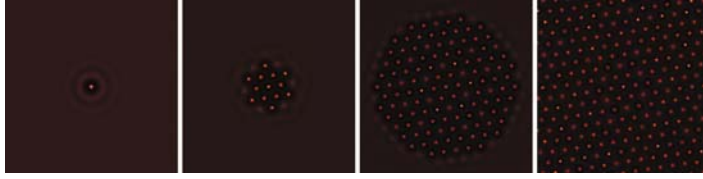


Fig. 3 Development of $m = 6$ azimuthal instability. From *left to right*: $t = 0, 100, 200, 300$. $\theta = 1.1$, $I = 0.97$

detuning. The ring surrounding the KCS core breaks into five or six spots, respectively. Numerical integration of (1) shows that the resulting structure then grows to invade the homogeneous background. For $\theta < 1.1$, the system is unstable to perturbations with azimuthal number $m = 6$, leading to a hexagonal pattern (Fig. 3). This pattern is not stationary but oscillates because of the values of I_s and θ [35]. For a narrow domain around $\theta = 1.2$ (Fig. 1), $m = 5$ dominates and the growing pattern, though locally hexagonal, retains its global five-fold symmetry (Figs. 4 and 5). Due to periodic boundary conditions, penta–hepta defects are created as soon as the pattern fills the whole system.

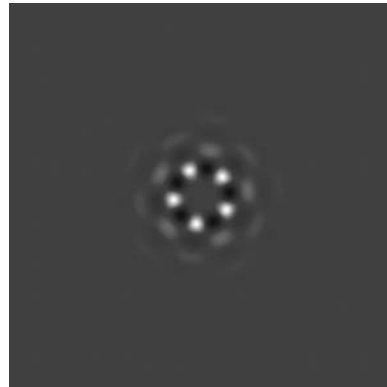


Fig. 4 Eigenmode corresponding to an azimuthal $m = 5$ instability. $\theta = 1.2$, $I = 0.95$

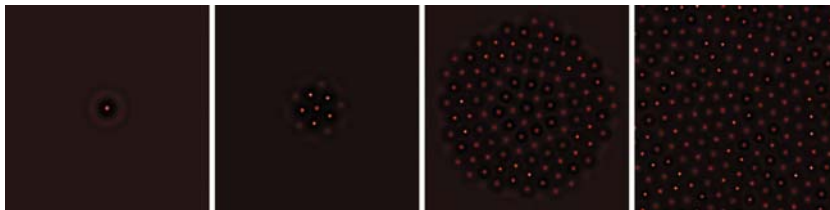


Fig. 5 Development of $m = 5$ azimuthal instability. From *left to right*: $t = 0, 200, 400, 600$. $\theta = 1.2$, $I = 0.95$

5 Oscillatory KCSs

The upper branch DS remains stable for a range of values of I_s , but undergoes a Hopf bifurcation when I_s is increased, leading to a limit cycle, and the DS oscillates autonomously [25, 31, 48]. The oscillatory regime is shown in parameter space in Fig. 1. Thus, in these conditions, a DS is an autonomous oscillon. An interesting connection to the conservative case is that the growth of the DS during the oscillations resembles the collapse regime observed for the 2D (or 2 + 1) NLSE. In this case, however, dissipation arrests this growth after some value is attained for the electric field, E . For one spatial dimension, Equation (1) also has DSs in the appropriate parameter regime, but these structures never undergo any Hopf instability.

As either the intra-cavity intensity, I_s , or the detuning, θ , is increased, the limit cycle gets closer and closer to the middle-branch KCS and the period of oscillation increases. This is illustrated in Fig. 6 for an increase in the detuning θ . The time evolution of the KCS maximum, as obtained from numerical integration of (1), is plotted in the left column, while the dashed line shows the maximum of the middle-branch KCS for comparison. The evolution in phase space, projected onto two variables, is sketched in the right column. At a critical value, θ_c , a global bifurcation

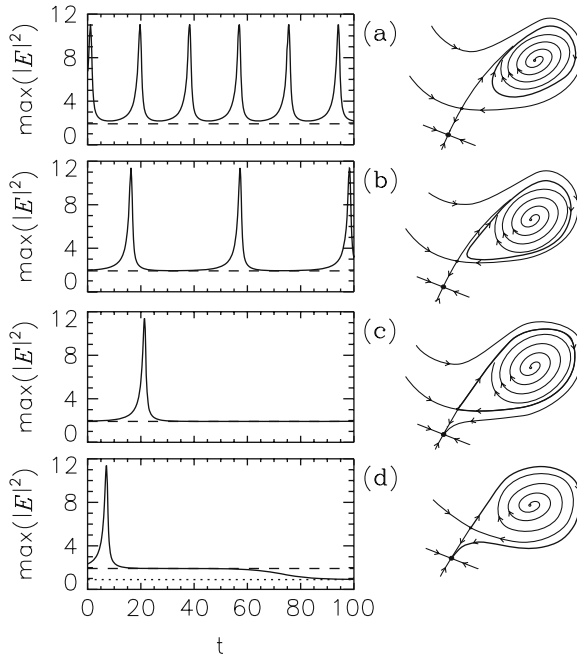
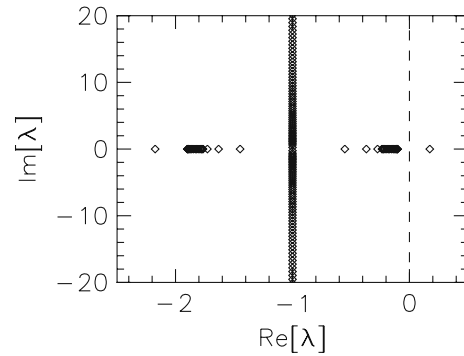


Fig. 6 *Left:* DS maximum intensity as a function of time for increasing values of the detuning parameter θ . From *top to bottom*: $\theta = 1.3, 1.3047, 1.30478592, 1.304788$. $I_s = 0.9$. *Right:* Sketch of the phase space for each parameter value. The *thick line* shows the trajectory of the DS in phase space

Fig. 7 Spectrum of the unstable (middle branch) DS for $\theta = 1.30478592$ and $I_s = 0.9$



takes place – the cycle touches the middle-branch KCS and becomes a homoclinic orbit [Fig. 6(c)].

It is perhaps surprising that the overall scenario can be understood qualitatively by resorting to a planar dynamical system, i.e., one with a 2D phase space. As we will show later, these two phase space variables correspond to the amplitude of localized modes of the system. The spectrum of eigenvalues for an unstable (middle) branch DS is shown in Fig. 7. There is only one positive eigenvalue, so this structure has a single unstable direction in the full phase space. The limit cycle corresponding to the oscillating KCS is such that it approaches the stable manifold of the middle-branch KCS and then escapes along the 1D unstable manifold. The middle-branch KCS is a saddle point in the reduced planar phase space. Once it is created, the middle-branch DS does not undergo any bifurcation for the parameter values explored here, and so remains a saddle point in phase space. When the limit cycle corresponding to the oscillating KCS touches the middle branch, the KCS undergoes a so-called *saddle-loop* bifurcation, and this is the subject of Sect. 6. An excitable regime, which will be described later in Sect. 8, emerges beyond this bifurcation.

6 Saddle-Loop Bifurcation

A saddle-loop bifurcation is a global bifurcation in which a limit cycle becomes bi-asymptotic to a (real) saddle point, or, in other words, becomes the homoclinic orbit of a saddle point (cf. [49, 50]), i.e., at criticality, a trajectory leaving the saddle point through the unstable manifold returns to it through the stable manifold. Thus, on one side of this bifurcation, one finds a detached limit cycle (stable or unstable), while on the other side, the cycle no longer exists, and only its *ghost* remains, as the bifurcation creates an exit slit that makes the system dynamics leave the region in phase space previously occupied by the cycle. (See the long plateau between $t = 15$ and $t = 60$ in Fig. 6(d).) Thus, after the bifurcation, the system dynamics jumps to another available attractor. In the present case, this alternative attractor is the homogeneous solution.

Let us take θ as the control parameter and assume that the saddle-loop bifurcation occurs for $\theta = \theta_{\text{SL}}$ and that $\theta < \theta_{\text{SL}}$ corresponds to the oscillatory side, where the limit cycle is detached from the saddle point, while, in turn, $\theta > \theta_{\text{SL}}$ corresponds to the side where the limit cycle is no longer present and there is only one stable solution, which is a fixed point. The fact that the bifurcation is global implies that it cannot be detected locally (a local eigenvalue passing through zero), but one can still resort to the Poincaré map technique¹ to analyze it, and, interestingly, the main features of the bifurcation can be understood from knowledge of the linear eigenvalues of the saddle.

The case studied here is the simplest: a saddle point with real eigenvalues, say $\lambda_s < 0$ and $\lambda_u > 0$, in a 2D phase space. Strictly speaking, in our case, the saddle has an infinite number of eigenvalues (Fig. 7), but only two eigenmodes take part in the dynamics close to the saddle. This will be studied in more detail in Sect. 7. It is convenient to define the so-called *saddle index* $\nu = -\lambda_s/\lambda_u$ and *saddle quantity* $\sigma = \lambda_s + \lambda_u$. It can be shown² that this cycle is stable for $\sigma < 0$, or $\nu > 1$, at the side of the saddle-loop bifurcation where one has a detached cycle, while for $\sigma > 0$ ($\nu < 1$), the cycle is unstable. Analogously, one can study the period of the cycle close to this bifurcation, and, to leading order, it is given by [51]

$$T \propto -\frac{1}{\lambda_u} \ln |\theta - \theta_{\text{SL}}|. \quad (7)$$

This expression is accurate for θ close enough to θ_{SL} . Interestingly, the transient time spent by a trajectory in the ghost region after the cycle has ceased to exist, close enough to the bifurcation point, also shows this scaling.

Numerically, the bifurcation point will be characterized by the fact that, on approaching it from the oscillatory side, the period will diverge to infinity (see Fig. 8 (a)) and also because, past this bifurcation point, the DS disappears and the system relaxes to the homogeneous solution, as shown in Fig. 6. For $I_s = 0.9$, the saddle loop takes place at $\theta_{\text{SL}} = 1.30478592$. In Fig. 6, the time evolution of the maximum of the DS is plotted for two values of the detuning, differing by 10^{-7} , with one just above and the other just below θ_{SL} . Figure 8 (b) displays a log-linear plot of the period versus a control parameter. As expected, it exhibits a linear slope. Furthermore, one can compare the value of the slope obtained from the simulations with its theoretical prediction, equation (7), namely $-1/\lambda_u$. The full spectrum of the

¹ The Poincaré map can be constructed through two cross-sections, i.e., two planes that are transversal to the limit cycle and that are placed slightly before and after the closest approach of the cycle to the saddle point. One can construct two maps from these two planes. The first is the so-called local (or linear or singular) map, T_0 , that takes the flow from the plane before the saddle point to the plane after the saddle point, and is dominated by the saddle point. The second is the global (or nonlinear) map, T_1 , that takes the flow all the way from the plane, past the saddle point through all of the limit cycle back to the plane before the saddle point. The complete Poincaré map is the composition of these two maps. It has to be remarked that the T_0 map is unbounded, as the return time is infinity at the onset of the global bifurcation.

² For details refer, e.g., to Sect. 12.3 of [49].

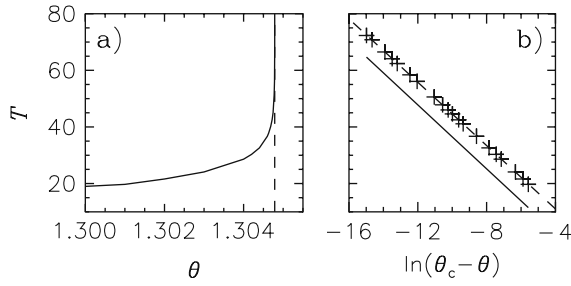


Fig. 8 (a) Period of the limit cycle, T , as a function of the detuning, θ , for $I_s = 0.9$. The vertical dashed line indicates the threshold of the saddle-loop bifurcation, $\theta_c = 1.30478592$. (b) Scaling of the period in the saddle-loop bifurcation. Crosses correspond to numerical simulations, while the solid line, arbitrarily positioned, has a slope $-1/\lambda_u$, with $\lambda_u = 0.177$, obtained from the stability analysis of the middle-branch KCS

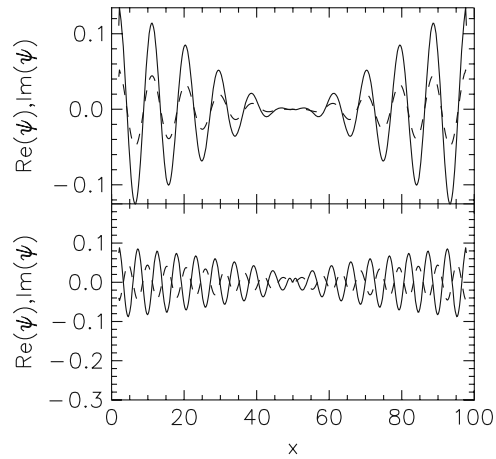
middle-branch soliton for $\theta = \theta_{SL}$ is shown in Fig. 7. The agreement between the simulations and theoretical slopes is within 1%.

A comment is in place here regarding the spectrum shown in Fig. 7. The spectrum is formed by a stable continuous spectrum (although numerically discretized) and a discrete one with a positive ($\lambda_u = 0.177$) and a negative ($\lambda_s = -2.177$) eigenvalue. Having this spectrum in mind, it is perhaps surprising that one can describe the bifurcation route very well qualitatively, and to some extent quantitatively (cf. the observed scaling law, Fig. 8), by resorting to a planar dynamical system when many modes could, in principle, be involved. The first mode of the planar theory unequivocally corresponds to the positive (unstable) eigenvalue, $\lambda_u = 0.177$, while, in first approximation, the second mode should correspond to the second nearest to zero eigenvalue. However, this eigenvalue belongs to a continuum band, and the arbitrarily close eigenvalues of its band could play a role in the dynamics, modifying the planar theory. Moreover, considering this mode, $\lambda \sim -0.10$, the saddle index $\nu = -\lambda/\lambda_u < 1$, indicating that the cycle emerging from the saddle loop should be unstable, although we observe otherwise. The analysis of the modes of the unstable DS and dimensionality of the phase space is addressed in detail in the next section.

7 Quantitative Phase Space Projection

We now study the dynamics in terms of the modes obtained when performing the stability analysis of the middle-branch DS in a parameter region close to the saddle-loop bifurcation. By plotting the spatial profile of the modes, one obtains a clue to identifying the relevant modes for the dynamics. It turns out that most of the modes of the stable spectrum are delocalized. Figure 9 contains a representation of two such delocalized modes. The bands of extended modes correspond to modes of the homogeneous background, and are basically Fourier modes, apart from a radial dependence coming from the fact that we are using radial instead of

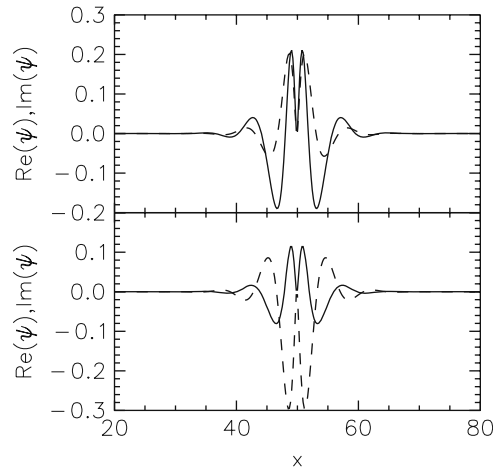
Fig. 9 Stable extended modes from the continuous band. The *top (bottom) panel* shows the transverse cut of the mode associated with the eigenvalue $\lambda = -0.1$ ($\lambda = -1 + i0.24$) of Fig. 7. The *solid (dashed) line* indicates the real (imaginary) part of the eigenmode



Cartesian coordinates. As illustrated in Fig. 9, the basic difference between these modes is the wavenumber of their oscillations. There are, however, two exceptions, viz. two localized modes which are the one corresponding to the unstable direction and the most stable mode (which has eigenvalue $\lambda_s = -2.177$). Figure 10 displays the spatial profiles of these two modes. The fact that the dynamics of the DS remains localized in the space indicates that only these two localized modes take part in the dynamics.

Using this knowledge of the spectrum and the relevant eigenmodes, we can now explain the stability of the orbits emerging out of the bifurcation, specifically by employing the saddle index introduced above. Computing this index for the two modes that participate in the saddle-loop bifurcation, one obtains $\nu = 2.177/0.177 > 1$, and this fits perfectly with the fact that the cycle that detaches at one side of the

Fig. 10 Transverse cut of the unstable (*top*) and the most stable (*bottom*) modes of the unstable DS. These modes are associated with the eigenvalues $\lambda_u = 0.177$ and $\lambda_s = -2.177$ of Fig. 7, respectively. The *solid (dashed) line* indicates the real (imaginary) part of the eigenmode



bifurcation point is stable. Thus, one may understand that the whole dynamical instability scenario of the DS can be analyzed qualitatively in a planar dynamical system.

A closer inspection of the dynamics in the *linear* region, namely the region close to the saddle point, provides a justification of the role of the two participating localized modes – stable and unstable. Figure 6a contains a time trace of one such trajectory in the parameter region in which the limit cycle is stable, but close to the saddle-loop bifurcation. We project the deviation of the trajectory from the unstable DS onto the most stable and the unstable eigenvectors of the adjoint Jacobian matrix of the middle-branch KCS. These projections are the amplitudes of the unstable (β_1) and the most stable (β_2) modes, whose profiles are shown in Fig. 10. In the linear region close to the saddle point, the amplitudes of the other modes are negligible. The trajectory enters the linear region through the stable mode and leaves the region through the unstable one. This behavior is clear in the insets of Fig. 11. Next, we reconstruct the qualitative sketch of the bifurcation shown in Fig. 6 from our knowledge of the projections onto the modes, that is, we represent the trajectories before and after the saddle-loop bifurcation in mode space. Thus, Fig. 11 contains a quantitative, reconstructed, 2D phase space from the two localized modes involved in the transition for a set of parameter values in the oscillatory (a) and excitable (b) sides of the transition. The dynamics takes place on a plane when close to the saddle, but, away from it, the nonlinear dynamics bends the trajectory out of the plane into a higher-dimensional space which produces the apparent crossing of the trajectory in Fig. 11.

This is the final numerical confirmation that the infinite-dimensional dynamical system on which DSs live can be reduced to a 2D dynamical system with an excellent degree of precision, and that the picture is fully consistent with a saddle-loop bifurcation.

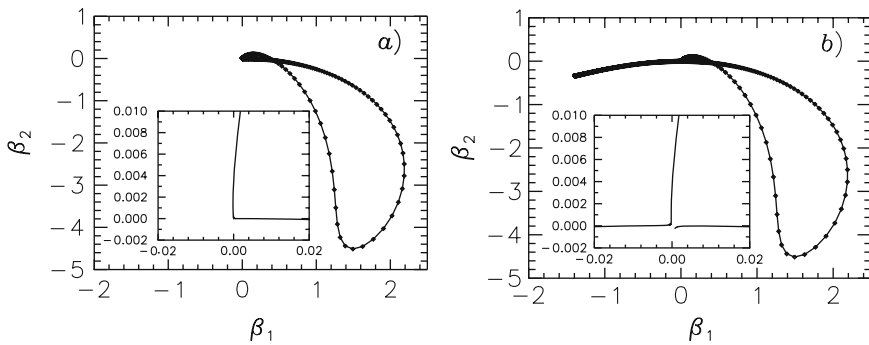


Fig. 11 Phase plane reconstructed by finding the amplitude of the deviation of the trajectory from the unstable DS in the unstable (β_1) and the most stable (β_2) modes of the middle-branch KCS. (a) Oscillatory trajectory ($\theta = 1.3047859$). (b) Excitable trajectory ($\theta = 1.3047860$). The symbols are equally time-spaced along the trajectory, so sparse symbols indicate fast dynamics while dense symbols indicate slow dynamics. The saddle point is at $(0, 0)$. The inset is a close-up of the linear region around the saddle

8 Excitable Behavior

The saddle-loop bifurcation described above involves a fixed point (the homogeneous solution) on one side of the bifurcation and an oscillation on the other, so the system is a candidate for exhibiting excitability [9]. While excitability as a result of a saddle-loop bifurcation has been observed in different systems [7, 8, 9], it should be noted that it does not always appear. In particular, one needs a fixed point attractor that is close enough to the saddle point that destroys the oscillation. The excitability threshold in this type of system is the stable manifold of the saddle point, which implies that the observed behavior is formally “Class I excitability” [9]. This means that the excitability is characterized by response times that can be infinite (if a perturbation exactly hits the stable manifold of the fixed point), or, conversely, frequencies can start from zero. In our system, the excitable threshold reduces by increasing I_s (Fig. 2), since the middle-branch KCS (the saddle point) gets progressively closer to the homogeneous solution (fixed point).

This excitability scenario was first shown in [28], and, in parameter space, it is found in the region above the dashed line corresponding to the saddle-loop bifurcation shown in Fig. 1. Figure 12 shows the resulting trajectories after applying a localized perturbation in the direction of the unstable DS with three different amplitudes

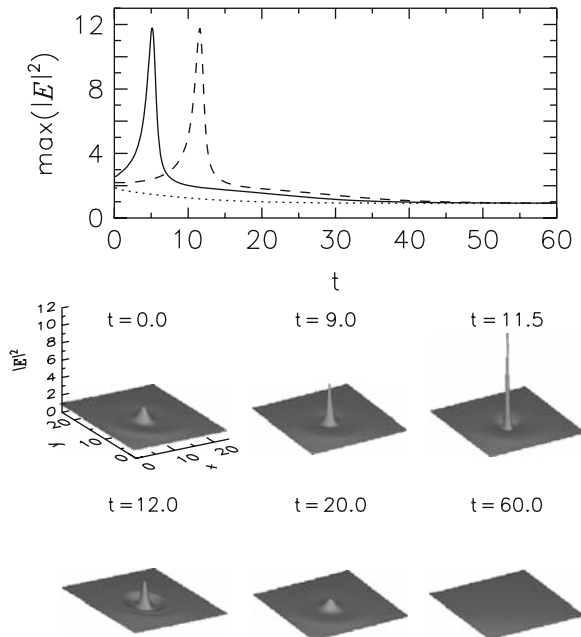


Fig. 12 *Top panel:* Time evolution of the maximum intensity, starting from the homogeneous solution ($I_s = 0.9$) plus a localized perturbation of the form of the unstable DS multiplied by a factor a . The *dotted*, *dashed*, and *solid lines* correspond to $a = 0.8$, $a = 1.01$, and $a = 1.2$, respectively. The 3D plots show the transverse profile at different times for $a = 1.01$

– one is below the excitability threshold (dotted line), while two are above it; of these, one is very close to threshold (dashed line) and the other is well above it (solid line). For the below-threshold perturbation, the system decays exponentially to the homogeneous solution, while, for the above-threshold perturbations, a long excursion in phase space is performed before returning to the stable fixed point. The refractory period for the perturbation just above the excitability threshold is appreciably longer, due to the effect of the saddle. The spatio-temporal dynamics of the excitable DS is also shown in Fig. 12. After an initial localized excitation is applied, the peak grows to a large value until the losses stop it. Then it decays exponentially until it disappears. A remnant wave dissipating the remaining energy is emitted out of the center.

It should be emphasized that, on neglecting the spatial dependence, equation (1) does not present any kind of excitability. The excitable behavior is an emergent property of the spatial dependence and it is strictly related to the dynamics of the 2D DS. The self-focusing collapse of the 2D NLSE is behind the long excursion in phase space. When a localized perturbation concentrates enough power, the self-focusing nonlinear mechanism induces a concentration of energy at that place. The presence of losses prevents collapse, the perturbation is finally dissipated, and the system returns to the homogeneous solution.

In parameter space, the excitable region is relatively large, as shown in Fig. 1. Therefore, it is potentially easy to observe experimentally. The excitable behavior belongs to Class I, as the period diverges to infinity when a perturbation hits the saddle. However, due to the logarithmic scaling law for the period, the parameter range over which the period increases dramatically is extremely narrow (see Fig. 8), so, from an operational point of view, systems exhibiting this scenario might not be classified as “Class I excitable”, as the large period responses may easily be missed [52].

9 Takens–Bogdanov Point

The saddle-loop (or homoclinic) bifurcation is, in some sense, not *generic*, namely, a tangency between a limit cycle and a saddle point which occurs exactly so that it happens simultaneously at both sides of the stable and unstable manifolds is, in principle, not to be expected generically. In fact, also due to the fact that global bifurcations are not always easy to detect, the most convincing argument for the existence of such bifurcations is to show that a dynamical system exhibits a certain type of co-dimension-2 point.

A scenario in which the unfolding of a co-dimension-2 point yields a saddle-loop (or homoclinic) bifurcation is a Takens–Bogdanov (TB) point [46, 53]. This is a double-zero bifurcation point in which a saddle-node bifurcation line and the zero-frequency limit of a Hopf bifurcation line (hence no longer a Hopf line at the crossing point) meet in a two-parameter plane. The particular feature that the Hopf line has zero frequency at the TB point allows this co-dimension-2 bifurcation to

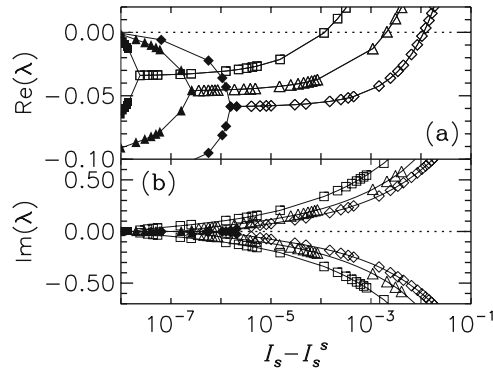
AU: Please check whether the edit of “The saddle-loop generically” is Ok.

occur in a 2D phase space. This bifurcation has to be distinguished from the occurrence of a crossing between a saddle-node and a Hopf line at non-zero frequency, known as Gavrilov-Guckenheimer or saddle node-Hopf point, which requires a 3D phase space to take place. One can prove that, from the unfolding of a TB point, a saddle-loop line, apart from the saddle-node and Hopf lines, emerges [46, 53] from the TB point.

This can be checked in Fig. 1, where a two-parameter bifurcation plot is presented as a function of the two parameters of the system, I_s and θ . The problem here is that the saddle-node and Hopf lines tend to meet only asymptotically, namely when $\theta \rightarrow \infty$. We had previously checked, in [28], that the distance between the saddle-node and the Hopf lines decreases as one increases θ . (The same happens with the saddle-loop line.) By calculating the eigenvalues, it can be seen that the frequencies (viz. their imaginary parts) do indeed go to zero as one approaches the TB point. Figure 13 displays the two eigenvalues of the upper-branch DS, with largest real parts for parameter values corresponding to three vertical cuts of Fig. 1. Open symbols correspond to eigenvalues with a non-zero imaginary part, while filled symbols are associated with real eigenvalues. The point where the open symbols cross zero in the upper panel of Fig. 13 signals the Hopf bifurcation, while the point where the filled symbols cross zero signals the saddle-node bifurcation. The origin for the three plots is taken as the saddle-node bifurcation. At some point along the branch of the two complex conjugate eigenvalues associated with the Hopf bifurcation, the imaginary part vanishes, leading to two branches of real eigenvalues, the largest of which is precisely the one responsible for the saddle-node bifurcation. As detuning increases, the Hopf and saddle-node bifurcation points get closer and closer, but the structure of the eigenvalues remains unchanged, so that when the Hopf and saddle-node bifurcations finally meet, the Hopf bifurcation has zero frequency, signaling a TB point.

The TB point appears asymptotically in the limit of large detuning, θ , and small pump, E_0 . In this limit, equation (1) becomes the conservative NLSE [31]. The Hopf instability in this limit was studied in [48], where evidence for a double-zero bifurcation point was given; however, the unfolding leading to the scenario presented here was not analyzed.

Fig. 13 Real part (*upper panel*) and imaginary part (*lower panel*) of the eigenvalues corresponding to the stable DS for three vertical cuts in Fig. 1, corresponding to three different values θ : squares, 1.7; triangles, 1.5; rhombs, 1.4, versus the difference between I_s and its value at the saddle-node bifurcation, $I_s - I_s^s(\theta)$



10 Effect of an Addressing Gaussian Beam

We now consider a pump consisting of a narrow Gaussian addressing beam on top of a homogeneous background. This is motivated by the fact that the common way to write and erase solitons in nonlinear cavities is by means of an addressing beam. This beam is customarily applied during a prescribed short interval of time. Here, we consider applying such a perturbation in a sustained way in order to control the spatial position of a soliton and its susceptibility to be excited. Hence, we consider a pump beam of the form $E_1(r) = E_0 + H \exp(-r^2/r_0^2)$, where E_0 is a homogeneous field, assumed real, H the height of the Gaussian perturbation, and r_0 its width. For convenience, we write the height of the Gaussian beam as

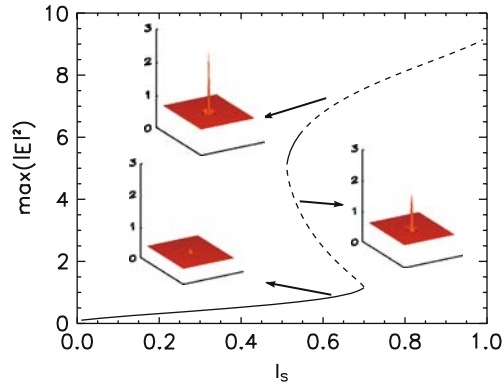
$$H = \sqrt{(I_s + I_{sh}) [1 + (\theta - I_s - I_{sh})^2]} - E_0, \quad (8)$$

where $I_s + I_{sh}$ would correspond to the intra-cavity field intensity of a cavity driven by a homogeneous field with an intensity equal to the intensity at the top of the Gaussian beam, $E_1 = E_0 + H$. This directly relates the height of the Gaussian beam, H , to a more intuitive quantity such as the equivalent intra-cavity intensity for a homogeneous pump.

The control parameters are the intra-cavity background intensity, I_s , the detuning, θ , and I_{sh} , which is associated with the Gaussian beam. Now the translational symmetry of the system (and also of its solutions) is broken, and the fundamental solution, which is no longer homogeneous, exhibits a bump which is small (when compared to the true DS), and this is the system response to the Gaussian perturbation. The bifurcation diagram for fixed I_{sh} and θ is given in Fig. 14.

On comparing Fig. 14 with the bifurcation diagram for a homogeneous pump (Fig. 2), it is clear that one feature which has changed is the region around the modulational instability point which signals the instability of the fundamental solution, i.e., the right end of the bistability region. In the homogeneous case, this instability occurs exactly at $I_s = 1$, but the introduction of a localized pump makes this point shift to a lower value (around $I_s = 0.7$ for these parameter values). One can also

Fig. 14 Bifurcation diagram, $\max(|E|^2)$ vs. I_s , for homogeneous pump plus Gaussian addressing beam ($I_{sh} = 0.7$) for $\theta = 1.34$. *Solid lines* represent stable solutions and *dashed lines* unstable ones. The 3D plots show, from top to bottom, the profiles of the upper-branch KCS, the unstable middle-branch KCS, and the fundamental solution, which is no longer homogeneous



notice that no line is plotted for the localized pump case, while, in the homogeneous case, the fundamental branch continues to exist as an unstable branch. This is because, in the latter case, the bifurcation has changed to a saddle-node bifurcation, in which the stable and unstable branches that meet at this point coalesce and disappear. This bifurcation is, in fact, a saddle node on the invariant circle (SNIC).

Exploring now the upper branch, past the (left) saddle-node bifurcation, a pair of stationary (stable, upper branch and unstable, middle branch) solutions are found, and they are not qualitatively different from those found in the homogeneous pump case. These two DS solutions are now slightly modified and fixed spatially (in the transverse plane) by the localized Gaussian beam, but their localized nature mainly comes from the self-focusing feature of the model, which implies that the DSs are self-sustained. On increasing I_s , the stable high-amplitude DS undergoes a Hopf bifurcation, resulting in a periodically oscillating DS. The oscillation is, however, destroyed for larger I_s in a saddle-loop bifurcation, leading to an excitable regime, in an analogous manner to what happens with a homogeneous pump. The saddle loop occurs at a value of I_s which is below the SNIC. The excitable regime is possible only while the fundamental solution exists (I_s between the saddle loop and the SNIC). After the SNIC, both the fundamental and the upper-branch DS are unstable, and a new, oscillatory, regime appears. Figure 15 shows the temporal evolution

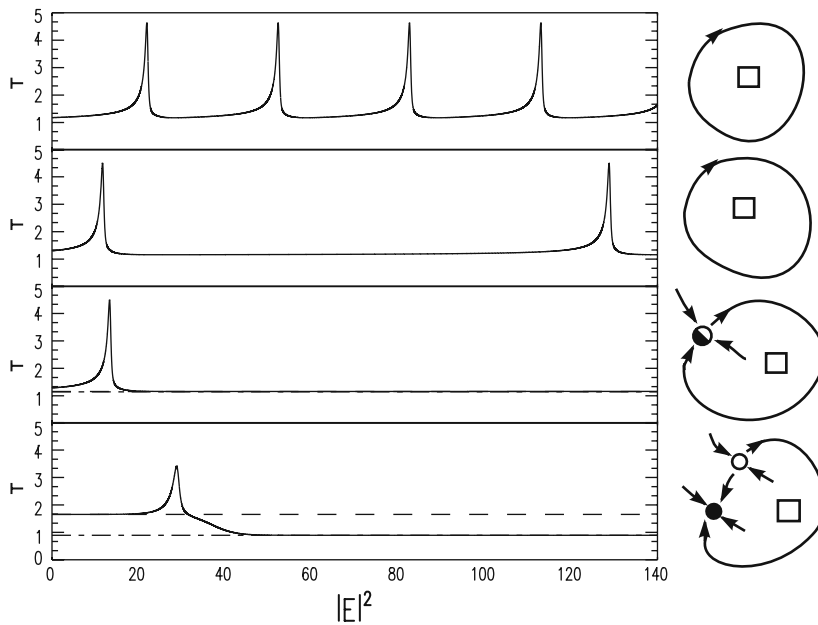


Fig. 15 Left: KCS maximum intensity, as a function of time, for decreasing values of I_s . From top to bottom, $I_s = 0.72, 0.7075, 0.707, 0.6$. $I_s h = 0.7$, $\theta = 1.34$. Right: sketch of the phase space for each parameter value. First two parameters correspond to region V (oscillating DS) in Fig. 16; the third one is very close to the SNIC bifurcation, while the fourth is in region IV (excitable), where this excitable behavior is dominated by the SNIC bifurcation

AU: In caption of Fig. 15 please confirm whether “ $I_s h$ ” can be changed to “ I_{sh} ”

in the new oscillatory regime. As I_s is decreased, the period of the oscillations becomes longer and it finally diverges on reaching the SNIC. The scaling of the period of oscillation shows that this is, in fact, a saddle node on the invariant circle (SNIC). A SNIC bifurcation induces excitable behavior for I_s below the critical value. This scenario is different from the previous one, although both lead to a regime where DSs are excitable. Here the excitable threshold can be controlled by the intensity of the addressing Gaussian beam that effectively causes the saddle and the stable fixed point to approach each other in phase space.

A better understanding of these instabilities can be gained through a two-parameter bifurcation diagram, Fig. 16, in which just one parameter is kept fixed, namely $\theta = 1.34$. (On the other hand, however, the structure of the branches cannot be seen in this diagram, as the electric field is not plotted. In this sense, these two representations, Figs. 14–16, have to be seen as complementary.) A first remark on this diagram is that the $I_{sh} = 0$ line must match the homogeneous case (Fig. 1). In the diagram shown in Fig. 16, the one-parameter bifurcation diagram in Fig. 14 corresponds to a cut along a vertical line located at $I_{sh} = 0.7$, and the saddle-node, Hopf, and saddle-loop bifurcation lines are found when going upward, followed by a final bifurcation line, viz. the SNIC. The sequence of behaviors exhibited by the system is as follows. Below the (left) saddle-node (SN) line, region I, the system has a single stationary (fundamental) solution, which has a small bump at the spatial region where the Gaussian pump is applied. On increasing I_s , a saddle point is created in a saddle-node bifurcation, along with another fixed point which is a DS (region II). Further on, this fixed point becomes unstable in an Andronov-Hopf bifurcation, and a cycle is created (region III). At this point, the stable fundamental solution and a stable cycle (oscillating DS) coexist in the system, together with the

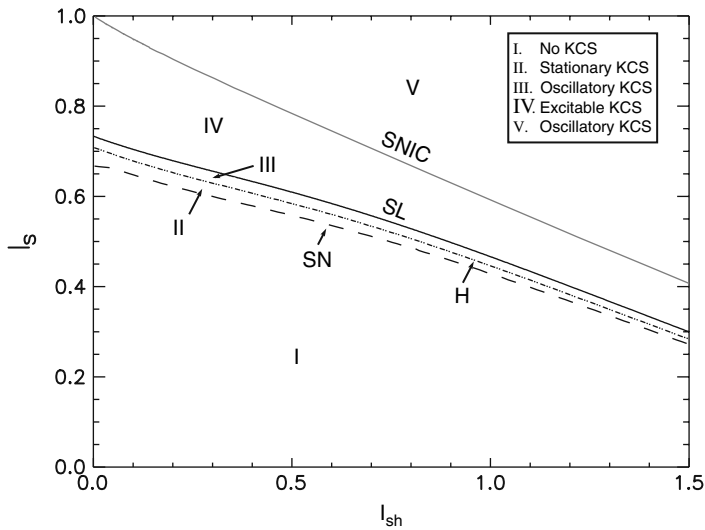


Fig. 16 Phase diagram I_s vs. I_{sh} for $\theta = 1.34$

unstable middle-branch KCS and the upper-branch KCS (which is now also unstable). If we further increase I_s , the limit cycle approaches the middle-branch KCS and collides in a saddle-loop bifurcation (SL line). Beyond this saddle loop, the fundamental solution becomes excitable in two possible ways (region IV). If the line indicated by SNIC is crossed, the fundamental solution (stable) and the lower DS stationary solution (saddle) annihilate each other inside an invariant circle, leading to oscillatory DS behavior (region V). Region IV is excitable in the sense that suitable perturbations of the fundamental solution lead to long excursions in phase space. This appears in two possible ways when changing system parameters depending on whether the SL or the SNIC bifurcation lines are crossed.

11 Concluding Remarks

We have analyzed the instabilities of dissipative solitons in a nonlinear Kerr cavity. Azimuthal instabilities lead to the destruction of the soliton, resulting in the formation of an extended pattern. On the other hand, instabilities occurring at zero azimuthal number lead to a localized structure whose amplitude oscillates in time, but in which the localized character of the soliton is preserved. More interestingly, beyond this oscillatory regime, an excitable regime, associated with the existence of dissipative structures, arises. This shows that, in order to exhibit excitability, extended systems do not necessarily require local excitable behavior. Instead, such phenomena can emerge because of spatial dependence through the dynamics of a coherent (localized) structure. This opens up the possibility of observing excitable behavior in a whole new class of systems where excitability was not thought to be present.

In Kerr cavities, there are two different mechanisms leading to excitability. One is based on a saddle-loop bifurcation in which a stable oscillating cavity soliton collides with an unstable one. The other occurs through a saddle node in the invariant circle (SNIC) bifurcation. The first one appears when either studying a homogeneous pump or considering a system pumped by a Gaussian beam on top of a homogeneous background, while the second mechanism appears only in the latter case. For both mechanisms, the excitability threshold is determined by the distance in phase space between the stable fixed point and the saddle. However, in the saddle-loop scenario, this distance cannot be easily tuned by changing system parameters, but, in the SNIC case, this distance vanishes precisely at the bifurcation point. By choosing to operate close to the SNIC bifurcation point, the threshold can be as low as desired. Therefore, it is possible to control the excitability threshold by changing a system parameter, e.g., the amplitude of the Gaussian addressing beam.

It has been shown that an excitable system can be used for computational purposes such as noise filtering or addition of input signals [54]. Thus, the excitable properties of cavity solitons open the possibility of optical information processing beyond the storage capabilities already suggested. This is a dynamical regime in which firing neuron-like structures could be generated at arbitrary points on the

AU: Please check whether the edit of “However, in the saddle-loop... point” is OK.

transverse plane of a nonlinear optical cavity. By coupling several of these *optical neurons*, reconfigurable optical networks could be created with the aim of processing information in a similar way to networks of neurons.

References

1. D. Murray, *Mathematical Biology*, (Springer, New York, 2002), Chap. 11.
2. E. Meron, Phys. Rep. **218**, 1 (1992).
3. H.J. Wünsche, O. Brox, M. Radziunas, and F. Henneberger, Phys. Rev. Lett. **88**, 023901 (2002).
4. S. Barland, O. Piro, M. Giudici, J.R. Tredicce, and S. Balle, Phys. Rev. E **68**, 036209 (2003).
5. J.L.A. Dubbeldam, B. Krauskopf, and D. Lenstra, Phys. Rev. E **60**, 6580 (1999).
6. B. Krauskopf, K. Schneider, J. Sieber, S. Wiczorek, and M. Wolfrum, Optics Commun. **215**, 367 (2003).
7. F. Plaza, M.G. Velarde, F.T. Arecchi, S. Boccaletti, M. Ciofini, and R. Meucci, Europhys. Lett. **38**, 85 (1997).
8. J. Rinzel and G.B. Ermentrout, in *Methods in Neuronal Modeling*, edited by C. Koch and I. Segev, (MIT Press, Cambridge, MA, 1989).
9. E.M. Izhikevich, Int. J. Bif. Chaos **10**, 1171 (2000).
10. Akhmediev, N., Ankiewicz, A. *Dissipative solitons*, Lect. Notes Phys. **661**. Springer, Berlin (2005)
11. O. Thual and S. Fauve, J. Phys. (France) **49**, 1829 (1988).
12. J.E. Pearson, Science **261**, 189 (1993).
13. K.J. Lee and H.L. Swinney, Science **261**, 192 (1993).
14. I. Müller, E. Ammelt, and H.G. Purwins, Phys. Rev. Lett. **82**, 3428 (1999).
15. N.N. Rosanov, *Progress in Optics*, (Elsevier, Amsterdam, 1996), Vol. **35**.
16. Feature Section on Cavity Solitons, edited by L.A. Lugiato, IEEE J. Quantum Electron. **39**, #2 (2003).
17. W.J. Firth and C.O. Weiss, Opt. Photon. News **13**, 55 (2002).
18. M. Tlidi, P. Mandel, and R. Lefever, Phys. Rev. Lett. **73**, 640 (1994).
19. S. Barland, et al., Nature (London) **419**, 699 (2002).
20. W.J. Firth and A.J. Scroggie, Phys. Rev. Lett. **76**, 1623 (1996).
21. P. Couillet, C. Riera, and C. Tresser, Phys. Rev. Lett. **84**, 3069 (2000).
22. P. Couillet, C. Riera, and C. Tresser, Chaos **14**, 193 (2004).
23. P.B. Umbanhowar, F. Melo, and H.L. Swinney, Nature (London) **382**, 793 (1996).
24. W.J. Firth, A. Lord, and A.J. Scroggie, Physica Scripta **67**, 12 (1996).
25. W.J. Firth, G.K. Harkness, A. Lord, J.M. McSloy, D. Gomila, and P. Colet, J. Opt. Soc. Am. B **19**, 747 (2002).
26. S. Longhi, G. Steinmayer, and W.S. Wong, J. Opt. Soc. Am. B **14**, 2167 (1997).
27. V.K. Vanag and I.R. Epstein, Phys. Rev. Lett. **92**, 128301 (2004).
28. D. Gomila, M.A. Matías, and P. Colet, Phys. Rev. Lett. **94**, 063905 (2005).
29. D. Gomila, A. Jacobo, M.A. Matías, and P. Colet, Phys. Rev. E, **75**, 026317 (2007).
30. C. Sulem and P.L. Sulem, *The Nonlinear Schrödinger Equation*, (Springer, New York, 1999).
31. W.J. Firth and A. Lord, J. Mod. Optic. **43**, 1071 (1996).
32. L.A. Lugiato and R. Lefever, Phys. Rev. Lett. **58**, 2209 (1987).
33. J.J. Rasmussen and K. Rypdal, Phys. Scr. **33**, 481 (1986).
34. M.V. Goldman, K. Rypdal, and B. Hafizi, Phys. Fluids **23**, 945 (1980).
35. D. Gomila, and P. Colet, Phys. Rev. A **68**, 011801 (R) (2003).
36. R. Montagne, E. Hernández-García, A. Amengual, and M. San Miguel, Phys. Rev. E **56**, 151 (1997).
37. A.J. Scroggie, Chaos, Soliton, Fract. **4**, 1323 (1994).

38. P.D. Woods, and A.R. Champneys, *Physica D* **129**, 147 (1999).
39. T. Maggipinto, M. Brambilla, G.K. Harkness, and W.J. Firth, *Phys. Rev. E* **62**, 8726 (2000).
40. B. Schäpers, M. Feldmann, T. Ackemann, and W. Lange, *Phys. Rev. Lett.* **85**, 748–751 (2000).
41. B. Schäpers, T. Ackemann, and W. Lange, *Proc. SPIE* **4271**, 130 (2001).
42. A. Schreiber, B. Thüering, M. Kreuzer, and T. Tschudi, *Optics Commun.* **136**, 415 (1997).
43. V.B. Taranenko, I. Ganne, R.J. Kuszelewicz, and C.O. Weiss, *Phys. Rev. A* **61**, 063818 (2000).
44. W.J. Firth, and G.K. Harkness, *Asian J. Phys.* **7**, 665 (1998).
45. G.-L. Oppo, A.J. Scroggie, and W. Firth, *Phys. Rev. E* **63**, 066209 (2001).
46. Y.A. Kuznetsov, *Elements of Applied Bifurcation Theory*, 2nd ed., (Springer, New York, 1998).
47. J.M. McSloy, W.J. Firth, G.K. Harkness, and G.L. Oppo, *Phys. Rev. E* **66**, 046606 (2002)
48. D.V. Skryabin, *J. Opt. Soc. Am. B* **19**, 529 (2002).
49. P. Glendinning, *Stability, Instability, and Chaos*, (Cambridge U.P., Cambridge, UK, 1994).
50. S. Wiggins, *Global Bifurcations, and Chaos: Analytical Methods*, (Springer, New York, 1988).
51. P. Gaspard, *J. Phys. Chem.* **94**, 1 (1990).
52. E.M. Izhikevich, *Dynamical Systems in Neuroscience*, (MIT Press, Cambridge, MA, 2006).
53. J. Guckenheimer, and P. Holmes, *Nonlinear Oscillations, Dynamical Systems, and Bifurcations of Vector Fields*, (Springer, New York, 1983).
54. C. Koch, *Biophysics of Computation: Information Processing in Single Neurons*, (Oxford U.P., New York, 1998).